

RESEARCH LETTER

10.1002/2016GL071560

Key Points:

- We simulated tensile and shear failure within idealized glaciers using a full-Stokes ice dynamics model
- Surface and basal crevasses intersect when rapidly sliding glaciers thin to buoyancy, and shear failure occurs when ice thickness is large
- Tensile and shear failure mechanisms together provide lower and upper bounds on permissible ice thickness for any given water depth

Supporting Information:

- Text S1
- Table S1

Correspondence to:

Y. Ma,
yuema@umich.edu

Citation:

Ma, Y., C. S. Tripathy, and J. N. Bassis (2017), Bounds on the calving cliff height of marine terminating glaciers, *Geophys. Res. Lett.*, 44, 1369–1375, doi:10.1002/2016GL071560.

Received 21 OCT 2016

Accepted 12 JAN 2017

Accepted article online 19 JAN 2017

Published online 4 FEB 2017

Bounds on the calving cliff height of marine terminating glaciers

Yue Ma¹, Cory S. Tripathy², and Jeremy N. Bassis³

¹Physics Department, University of Michigan, Ann Arbor, Michigan, USA, ²Earth and Environmental Sciences, University of Michigan, Ann Arbor, Michigan, USA, ³Climate and Space Sciences and Engineering, University of Michigan, Ann Arbor, Michigan, USA

Abstract Increased calving and rapid retreat of glaciers can contribute significantly to sea level rise, but the processes controlling glacier retreat remain poorly understood. We seek to improve our understanding of calving by investigating the stress field controlling tensile and shear failure using a 2-D full-Stokes finite element model. Using idealized rectangular geometries, we find that when rapidly sliding glaciers thin to near buoyancy, full thickness tensile failure occurs, similar to observations motivating height-above-buoyancy calving laws. In contrast, when glaciers are frozen to their beds, basal crevasse penetration is suppressed and calving is minimal. We also find that shear stresses are largest when glaciers are thickest. Together, the tensile and shear failure criteria map out a stable envelope in an ice-thickness-water-depth diagram. The upper and lower bounds on cliff height can be incorporated into numerical ice sheet models as boundary conditions, thus bracketing the magnitude of calving rates in marine-terminating glaciers.

1. Introduction

Observations show that the Greenland and Antarctic ice sheets are now losing mass at an accelerating rate [e.g., *Vaughan et al.*, 2013]. Currently, about half of the observed mass loss from ice sheets is controlled by iceberg calving [e.g., *Depoorter et al.*, 2013; *Khan et al.*, 2015; *Liu et al.*, 2015]. However, despite the need for more complete models of the dynamic processes associated with fracture propagation and iceberg detachment, the calving process remains poorly understood and there is no universal parameterization or calving law that applies to all regimes [*Benn et al.*, 2007a, 2007b; *Bassis*, 2011].

There are currently several approaches used to parameterize calving in ice sheet models. One of the oldest techniques seeks empirical correlations for a time-averaged “calving rate,” defined as the mean flux of ice lost due to iceberg calving. Promising correlations have been obtained between calving rate and ice thickness [e.g., *Reeh*, 1968; *Amundson and Truffer*, 2010], water depth [e.g., *Brown et al.*, 1982; *Meier and Post*, 1987; *Pelto and Warren*, 1991; *Hughes*, 1992], strain rate [e.g., *Alley et al.*, 2008; *Levermann et al.*, 2012], or height above buoyancy [e.g., *Sikonia*, 1982; *van der Veen*, 1996]. However, these correlations only apply to limited regimes and can fail when extrapolated beyond their domain of applicability. For example, models that assume calving rate is determined solely by water depth cannot account for the formation of floating ice tongues and ice shelves. Moreover, even when constrained to the regime for which they were derived, empirical correlations lack a physical basis, casting doubt on the validity of future predictions.

An alternative method seeks to model the physical processes that lead to calving events more directly. The most promising approach in this family involves methods that seek to predict the depth of surface and basal crevasses penetration, assuming that an iceberg will detach when surface and basal crevasses intersect and isolate an iceberg [e.g., *Benn et al.*, 2007b; *Nick et al.*, 2010; *Bassis*, 2011; *Bassis and Ma*, 2015]. Crevasse penetration depths are often computed assuming that crevasses penetrate to the depth where the tensile stress vanishes (e.g., the Nye zero stress model [*Nye*, 1955; *Benn et al.*, 2007a, 2007b; *Otero et al.*, 2010; *Nick et al.*, 2010; *Cook et al.*, 2012; *van der Veen*, 2013], Linear Elastic Fracture Mechanics [e.g., *Smith*, 1976; *van der Veen*, 1998, 2007; *Rist et al.*, 1999], or various flavors of continuum damage mechanics [e.g., *Pralong and Funk*, 2005; *Borstad et al.*, 2012; *Albrecht and Levermann*, 2012; *Duddu et al.*, 2013; *Albrecht and Levermann*, 2014; *Krug et al.*, 2014; *Bassis and Ma*, 2015; *Mobasher et al.*, 2016]).

Flow line models based on crevasse depths have been successful in reproducing glacier retreat [e.g., *Nick et al.*, 2010; *Cook et al.*, 2012]. These models, however, frequently use surface melt water-filled crevasses as a tuning parameter to match observations [e.g., *Nick et al.*, 2010; *Cook et al.*, 2012] or have invoked buoyant forces near the terminus [e.g., *James et al.*, 2014; *Wagner et al.*, 2016]. More recently, *Bassis and Walker* [2012] proposed that in addition to tensile failure, it is also possible for crevasses to propagate through shear failure. Based on thin-film approximations, *Bassis and Walker* [2012] and *Bassis et al.* [2017] were able to derive an upper bound on the ice thickness at the terminus of a glacier and is the basis for the “marine ice cliff instability” recently invoked as a mechanism that can lead to rapid disintegration of marine-based ice sheets [*Pollard and DeConto*, 2009; *DeConto and Pollard*, 2016].

In this study, we seek to examine the depth to which crevasses propagate by computing near-terminus stress fields using a (full) Stokes approximation that dispenses with the shallow approximation which limited several previous studies of the calving process. We use this model to examine the effect of the full stress regime on crevasse propagation in idealized slab geometries and generalize previous models by including the possibility for shear failure to explore conditions when full thickness glacier failure is likely to occur.

2. Model Description

2.1. Ice Dynamics

We solve the force balance equations along a central flow line that cuts vertically through the middle of a glacier. In the interest of simplicity, we neglect lateral shear and restrict our model domain to a flow line near the terminus of a glacier with x representing the along-flow coordinate and z representing the vertical coordinate. Denoting the components of the deviatoric stress tensor by τ_{ij} , pressure by p , density of ice by ρ , and gravitational acceleration by g , conservation of momentum can be written as follows:

$$\frac{\partial \tau_{xx}}{\partial x} + \frac{\partial \tau_{xz}}{\partial z} = \frac{\partial p}{\partial x} \quad (1)$$

$$\frac{\partial \tau_{xz}}{\partial x} + \frac{\partial \tau_{zz}}{\partial z} = \frac{\partial p}{\partial z} - \rho g \quad (2)$$

$$\frac{\partial u}{\partial x} + \frac{\partial w}{\partial z} = 0. \quad (3)$$

The rheology of ice is specified by the usual power law rheology [*Paterson*, 1994]. The glacier is traction free at the ice-air interface. At the ice-water interface, we insist on continuity of traction, assuming that ocean water is in hydrostatic equilibrium. We explore free-slip and no-slip (frozen) boundary conditions along the bottom of the glacier, allowing us to bracket the effect of basal resistance on our results. Because our primary interest is in grounded tidewater glaciers, we do not allow the ice to transition to a floating regime when it approaches buoyancy. For the upstream (inflow) boundary condition, we assume free slip in the vertical direction and no slip in the horizontal direction. In the free-slip case the model is translationally invariant and the zero inflow boundary condition amounts to the adoption of a reference frame moving at the same velocity as incoming ice (a Lagrangian reference frame). This is appropriate for our idealized (flat and even) bed, but including an upstream inflow velocity would be required if we had bed roughness or a velocity-dependent basal traction boundary condition. For the no-slip condition, the no inflow boundary condition is consistent with a locally determined ice flow associated with the shallow ice approximation. We supplement the continuum dynamics described above with two modes of failure: tensile and shear, which we describe next.

2.2. Tensile Failure

The first mode of failure corresponds to tensile failure and has received the most attention from the community. We simulate the penetration of surface and basal crevasses assuming that crevasses penetrate to the depth where the largest principal stress vanishes [e.g., *Nye*, 1955; *Benn et al.*, 2007a; *van der Veen*, 2013]. It is also possible to simulate crevasse depths using Linear Elastic Fracture Mechanics [e.g., *van der Veen*, 2013], but we prefer the Nye zero stress model because it more closely approximates the depth of closely spaced crevasses and is more appropriate for the viscous rheology [*Weertman*, 1973; *Benn et al.*, 2007a]. We can calculate the paths crevasses propagate along by calculating the eigenvector associated with the largest principal stress. To compute basal crevasse depths, we assume that basal crevasses near the terminus are connected to the ocean and thus filled by sea water. This neglects fluctuations in water pressure associated with

subglacial hydrology observed upstream from the calving front, but is likely a reasonable approximation very close to the calving front. We seed crevasses assuming glaciers have densely spaced preexisting flaws in the near-terminus region so that crevasses will always penetrate to the deepest portions of the glacier possible based on the stress field. Once the surface and basal crevasses connect with each other, we assume that a calving event occurs and the simulation is arrested.

2.3. Shear Failure

The second mode of failure we examine is shear failure, which occurs when the maximum shear stress exceeds the shear strength of ice. The shear strength of ice is not well constrained, but field and laboratory studies suggest values in the range of 500 kPa to 1 MPa [Horeth, 1948; Frederking *et al.*, 1988; Schulson, 1999; Petrovic, 2003; Bassis and Walker, 2012]. We use a value of 500 kPa in our model. We compute the maximum shear stress to determine when shear failure causes full thickness failure of the glacier, again assuming optimal placement of seeds for faults within the glacier and examining conditions in which faults span the entire ice thickness. Crucially, as noted by Bassis and Walker [2012], shear failure, unlike tensile failure, is more likely to occur in the interior of the glacier where compressive stresses remain large.

2.4. Initial Conditions and Numerical Implementation

We use the open source FEniCS package [Logg *et al.*, 2012; Alnæs *et al.*, 2015] to solve the stress equilibrium model. On day 0, each glacier was initialized as an (isothermal) rectangular slab on a flat bed with prescribed thickness and water depth, but no crevasses. Because our interest lies in the near-terminus region, we set the length-to-thickness ratio of the glacier in each simulation to 6 times to avoid edge effects associated with the upstream boundary condition, so that an increase in the ratio will not lead to any substantial changes in the stress field near the calving front. We use a mesh of triangular elements and a resolution of 1% of the initial glacier thickness uniformly in both vertical and horizontal directions. At this resolution our results are insensitive to a factor of 2 changes in resolution. During each time step (nominally 1 day), the glacier deforms and crevasses begin to propagate based on the evolving stress field. For a given stress field, we propagate crevasses until they extend to their maximum depth allowed. Restricted by the resolution of the model, crevasses can only propagate to discrete nodes, thus creating a slight zigzag in the simulated path. We also assume that crevasses are sufficiently narrow, that they have little effect on the stress field, and use the stress field diagnostically to deduce the depth of crevasses. Previous work using much more complex viscoelastic damage models suggest that this is a reasonable first-order approximation [Duddu *et al.*, 2013; Mobasher *et al.*, 2016]. At the end of each time step, we also remesh after advecting all the nodes along their own nodal velocity vector to maintain a constant mesh quality throughout the simulation, and the locations of existing crevasse paths are stored.

3. Results

3.1. Tensile Failure

We first initialized a set of glaciers with varying ice thickness and water depth combinations and allowed them to evolve until either surface and basal crevasse penetrated the entire ice thickness or crevasse penetration depths reached a steady state depth. Figures 1a, 1c, and 1e show a sequence of snapshots for one such example. In this simulation the glacier was initially 800 m thick terminating in 560 m deep water with a free-slip basal boundary condition. In the early stages of evolution, crevasses only penetrate about half of the ice thickness, but as the simulation proceeds and the glacier advances and thins, basal crevasses penetrate a larger fraction of the ice thickness. Eventually, the ice thickness approaches buoyancy and basal crevasses penetrate to the water line and intersect with surface crevasses, leading to a calving event. The final ice thickness ~ 700 m is comparable to the thickness of Helheim Glacier, where icebergs have been observed detaching as the glacier thins to near buoyancy [Joughin *et al.*, 2008]. Notably, unlike most previous models, we do not require melt water to fill crevasses to trigger a calving event.

This pattern of thinning to near buoyancy where basal crevasses intersect with surface crevasses was common to all simulations performed using a free-slip boundary condition. In contrast, when we performed the same simulations using a no-slip basal boundary condition, we found that surface crevasses penetrated deeper (Figures 2a and 2c) compared to the free-slip case, but the resulting compressive stress near the bed made it difficult for basal crevasses to form. A consequence of this is that surface and basal crevasses never penetrated the entire ice thickness and no calving events occurred in these simulations. This suggests that rapid sliding is a prerequisite for vigorous calving, which is broadly consistent with observations.

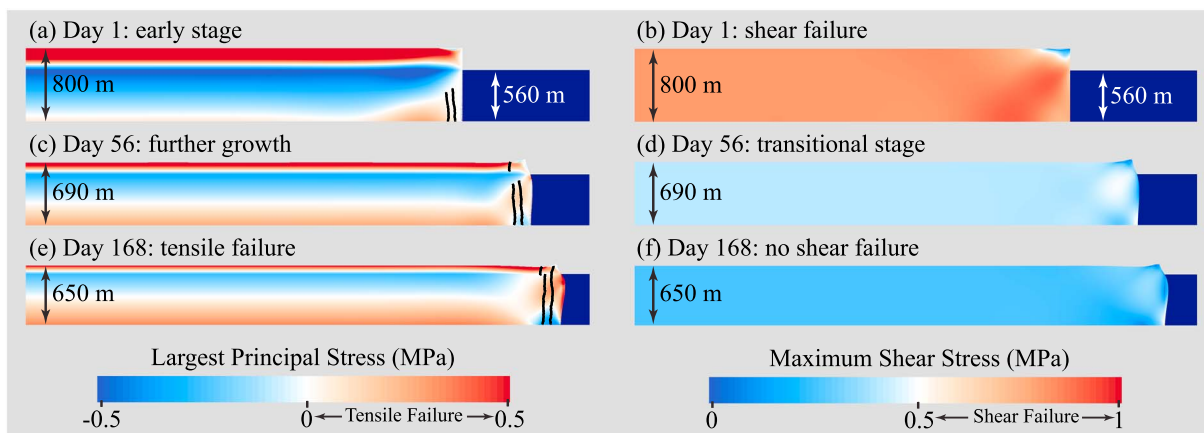


Figure 1. Snapshots showing the evolution of stresses and crevasse depths as a glacier advances and thins under free-slip basal boundary condition. (a, c, and e) The contours show the largest principal stress. Crevasse paths are denoted using black lines. (b, d, and f) The maximum shear stress. Figures 1a and 1b show the initial stage of an 800 m thick glacier terminating in 560 m water. Shear stresses are above the shear strength of ice almost everywhere. Figures 1c and 1d show the transitional stage during which the glacier has thinned to the point where shear stresses have decreased just beneath the shear strength of ice. In Figures 1e and 1f the glacier has thinned to near buoyancy and shear stresses are beneath the shear strength of ice, but surface and basal crevasses intersect and penetrate the entire ice thickness.

3.2. Shear Failure

We next examined the maximum shear stress for the same set of experiments. Figures 1b, 1d, and 1f show the same set of snapshots as in Figures 1a, 1c, and 1e but this time illustrate contours of the shear stress. In contrast to tensile stress, shear stress decreases as the glacier thins, as predicted by *Bassis and Walker* [2012]. We find that the thickest glacier configurations are most prone to failure (Figure 1b) but that the shear stress decreases as the glacier advances and thins until it becomes stable to shear failure (Figures 1d and 1f).

In contrast, Figures 2b and 2d show snapshots of shear stress with a no-slip boundary condition. Unlike the free-slip case, glacier configurations thicker than 500 m are unstable for all water depths, suggesting there is no stable ice cliff for glaciers thicker than 500 m. However, when near-terminus ice thicknesses is less than ~500 m, we see a pattern analogous to the free-slip case where shear stresses are largest for thick glaciers and decrease as the glacier thins. A larger yield strength would allow larger stable terminus thicknesses, but the qualitative pattern traced out remains the same.

3.3. Stability Regimes of Calving Glaciers

Combining the water depth and ice thickness measured in the model for marginal cases at the onset of tensile or shear failure, we obtain lower and upper “bounds” on the ice thickness for free-slip boundary conditions for a given yield strength. These combinations are shown in Figure 3 along with near-terminus ice thickness and water depth combinations obtained from IceBridge radar profiles [*Gogineni and Paden*, 2012]. The observational data provided by IceBridge flights span from 2006 to 2014 and include measurements of over 30 outlet glaciers across Greenland, most extensively the Helheim, Jakobshavn, Petermann, and

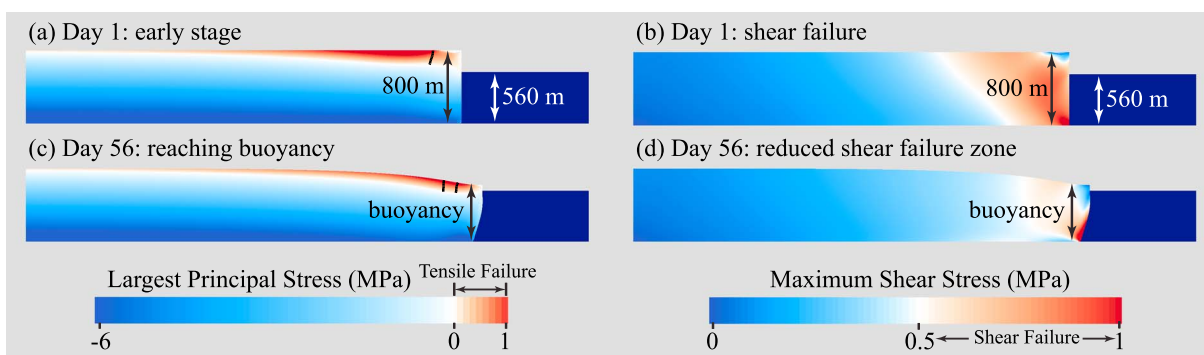


Figure 2. Snapshots showing the evolution of stresses and crevasses as a glacier advances and thins under no-slip basal boundary conditions. (a, c) The contours show the largest principal stress and black lines show crevasse paths; (b, d) maximum shear stress.

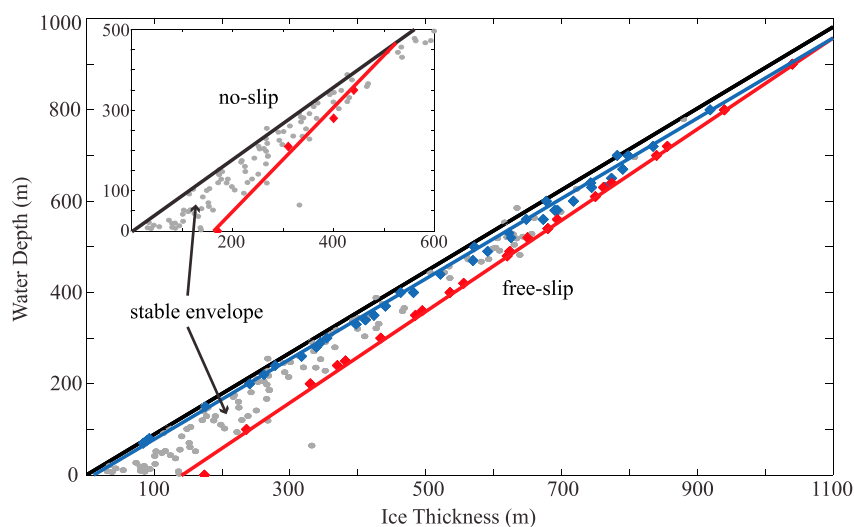


Figure 3. Upper and lower bounds on near-terminus ice thickness as a function of water depth for a free-slip basal boundary condition. The blue diamonds indicate ice thickness and water depth combinations when tensile failure triggered calving in simulations. Red diamonds indicate the threshold ice thickness when shear failure occurred in simulations. The blue and red lines are linear fits to the blue and red diamonds, respectively. Glaciers are stable between these two limits. The gray dots show observed ice thickness/water depth combinations. The black solid line traces out the maximum ice thickness for a given water depth before the glaciers become buoyant. Inset shows results for a no-slip basal boundary condition.

Hayes glaciers. These measurements were taken from Multichannel Coherent Radar Depth Sounder (MCoRDS): elevation of the radar, distance from the bottom of the glacier to the radar, and distance from the surface of the glacier to the radar, i.e., elevation, bottom, and surface, respectively. The water depth and ice thickness values used in Figure 3 are derived from the provided data, either a single radar measurement at the terminus or, more desirably, an average of the data over the span of 3 s at the terminus. Radar data in which the transition from ocean to outlet glacier is not clear, or inaccurate, are omitted from this study. More details about the observational data such as location, date of measurement, errors, etc. are provided in the supporting information (Table S1).

The lower limit on ice thickness suggests that surface and basal crevasses will intersect to isolate an iceberg when glaciers which experience little resistance from the bed (or lateral shear along the walls) approach buoyancy. In contrast, shear failure limits the ice thickness at the terminus to be less than ~ 150 m above the water line. These bounds compare well with observed water depth and ice thickness combinations detected in Greenland glaciers and deduced theoretically [Bassis and Walker, 2012], suggesting that glaciers occur in a narrow region of phase space of allowed ice thickness and water depth combinations.

Due to a lack of favorable conditions for tensile failure and a higher tendency for shear failure, the upper and lower bounds on the ice thickness for no slip are different from the free-slip case, as shown in Figure 3 inset. Above 500 m, thicker glaciers undergo shear failure and there is no stable ice thickness. For glaciers thinner than 500 m, crevasses never intersect, permitting a stable ice thickness up to and above buoyancy, allowing ice tongue formation.

4. Discussion

Our results suggest that crevasses penetrate through the entire ice thickness in glaciers that experience little resistance to flow from the bed or walls. This implies that rapidly sliding glaciers should rarely form floating ice tongues. Although (permanent) ice tongues are rarely observed in Alaska or other tidewater environments, floating ice tongues and ice shelves are prevalent in Antarctica and occur sporadically around Greenland [Meier and Post, 1987; van der Veen, 1996, 2002]. Our model would suggest that this requires glaciers with nonnegligible resistance to sliding along the bed or walls in the grounded portions of glaciers upstream of the grounding line. However, ancillary effects that we have not modeled (e.g., buoyancy forces and submarine melting) could also serve to affect ice tongue formation. In particular, our model does not yet include the

effect of submarine melting, which could alter the shape of the calving front along with the near-terminus stress field [e.g., *Truffer and Motyka, 2016*].

Our model also provides a physical explanation for the height-above-buoyancy calving law that has been found empirically to match observed retreat rates in many marine-terminating glaciers [*Sikonia, 1982; van der Veen, 1996*]. Our results imply that these glaciers must be sliding rapidly, which is consistent with the fact that glaciers undergoing vigorous calving tend to be rapidly flowing [e.g., *Benn et al., 2007a*]. Furthermore, our results highlight the prominent role that basal crevasses play in iceberg calving; dry surface crevasses alone can rarely penetrate deep enough to trigger calving. However, we do find that when surface crevasses penetrate to the waterline, they can intersect with basal crevasses, triggering a calving event, analogous to the criterion proposed by *Benn et al.* [2007a]. Although we have not considered water-filled surface crevasses, adding melt water to surface crevasses would cause calving to occur before buoyancy is reached, narrowing the range of the stable envelope. Hence, the presence of water in surface crevasses would increase the vulnerability of a glacier to iceberg calving and permit glaciers to calve before thinning to buoyancy.

5. Conclusions

The upper and lower bounds on ice thickness provided by our model can also be incorporated as boundary conditions into numerical models to bracket rates of glacier retreat [*Bassis et al., 2017*]. Moreover, our simulations suggest that glaciers can fail in both shear and tensile regimes and that these two different failure mechanisms provide bounds on permissible ice thickness for any given water depth. We also find that basal crevasses play a prominent role in calving in all simulations we conducted and that we do not need water-filled surface crevasses to initiate calving. Our simulations also provide an intuitive explanation for the height-above-buoyancy calving law that has successfully explained retreat in several environments. However, our model also shows that the height-above-buoyancy model is likely to breakdown if basal resistance becomes important. Finally, although our treatment of ice failure is very simple, the physical nature of the model suggests that it may be applied in a variety of models to yield useful constraints on permissible glacier geometries and simulate the rate at which glaciers retreat or advance.

Acknowledgments

This work was supported by National Science Foundation grant ANT 114085, National Oceanic and Atmospheric Administration, Climate Process Team: Iceberg Calving grant NA13OAR4310096, and National Science Foundation grant PLR-131568. We acknowledge the use of data and/or data products from CReSIS generated with support from the University of Kansas, NSF grant ANT-0424589, Operation IceBridge grant NNX16AH54G

References

- Albrecht, T., and A. Levermann (2012), Fracture field for large-scale ice dynamics, *J. Glaciol.*, *58*(207), 165–176.
- Albrecht, T., and A. Levermann (2014), Fracture-induced softening for large-scale ice dynamics, *Cryosphere*, *8*(2), 587–605.
- Alley, R. B., H. J. Horgan, I. Joughin, K. M. Cuffey, T. K. Dupont, B. R. Parizek, S. Anandakrishnan, and J. Bassis (2008), A simple law for ice-shelf calving, *Science*, *322*(5906), 1344–1344.
- Alnæs, M. S., J. Blechta, J. Hake, A. Johansson, B. Kehlet, A. Logg, C. Richardson, J. Ring, M. E. Rognes, and G. N. Wells (2015), The FEniCS project version 1.5, *Arch. Numer. Softw.*, *3*(100), doi:10.11588/ans.2015.100.20553.
- Amundson, J. M., and M. Truffer (2010), A unifying framework for iceberg-calving models, *J. Glaciol.*, *56*(199), 822–830.
- Bassis, J. N. (2011), The statistical physics of iceberg calving and the emergence of universal calving laws, *J. Glaciol.*, *57*(201), 3–16.
- Bassis, J. N., and Y. Ma (2015), Evolution of basal crevasses links ice shelf stability to ocean forcing, *Earth Planet. Sci. Lett.*, *409*, 203–211.
- Bassis, J. N., and C. C. Walker (2012), Upper and lower limits on the stability of calving glaciers from the yield strength envelope of ice, *Proc. R. Soc. A*, *468*(2140), 913–931.
- Bassis, J. N., S. V. Petersen, and L. M. Cathles (2017), Ice sheet collapse triggered by ocean forcing and modulated by isostatic adjustment, *Nature*, doi:10.1038/nature21069, in press.
- Benn, D. I., C. R. Warren, and R. H. Mottram (2007a), Calving processes and the dynamics of calving glaciers, *Earth Sci. Rev.*, *82*(3), 143–179.
- Benn, D. I., N. R. J. Hulton, and R. H. Mottram (2007b), 'Calving laws', 'sliding laws' and the stability of tidewater glaciers, *Ann. Glaciol.*, *46*(1), 123–130.
- Borstad, C. P., A. Khazendar, E. Larour, M. Morlighem, E. Rignot, M. P. Schodlok, and H. Seroussi (2012), A damage mechanics assessment of the Larsen B ice shelf prior to collapse: Toward a physically-based calving law, *Geophys. Res. Lett.*, *39*, L18502, doi:10.1029/2012GL053317.
- Brown, C. S., M. F. Meier, and A. Post (1982), Calving speed of Alaska tidewater glaciers, with application to Columbia glacier, *U.S. Geol. Surv. Prof. Pap.* 1258-C, U.S. Gov. Print. Off., Washington, D. C.
- Cook, S., T. Zwinger, I. Rutt, S. O'Neel, and T. Murray (2012), Testing the effect of water in crevasses on a physically based calving model, *Ann. Glaciol.*, *53*(60), 90–96.
- DeConto, R. M., and D. Pollard (2016), Contribution of Antarctica to past and future sea-level rise, *Nature*, *531*(7596), 591–597.
- Depoorter, M. A., J. L. Bamber, J. A. Griggs, J. T. M. Lenaerts, S. R. M. Ligtenberg, M. R. van den Broeke, and G. Moholdt (2013), Calving fluxes and basal melt rates of Antarctic ice shelves, *Nature*, *502*(7469), 89–92.
- Duddu, R., J. Bassis, and H. Waisman (2013), A numerical investigation of surface crevasse propagation in glaciers using nonlocal continuum damage mechanics, *Geophys. Res. Lett.*, *40*, 3064–3068, doi:10.1002/grl.50602.
- Frederking, R. M. W., O. J. Svec, and G. W. Timco (1988), On measuring the shear strength of ice, *Tech. Rep.*, Natl. Res. Council. Canada, Inst. for Res. in Constr., Canada.
- Gogineni, P., and J. Paden (2012), *CReSIS Radar Depth Sounder Data*, Digital Media, Lawrence, Kansas. [Available at <http://data.cresis.ku.edu/>]
- Horeth, J. M. (1948), Tensile strength and shear strength of ice, Master's thesis, Ann Arbor, Mich.
- Hughes, T. J. (1992), Theoretical calving rates from glaciers along ice walls grounded in water of variable depths, *J. Glaciol.*, *38*(129), 282–294.

- James, T. D., T. Murray, N. Selmes, K. Scharrer, and M. O'Leary (2014), Buoyant flexure and basal crevassing in dynamic mass loss at Helheim Glacier, *Nat. Geosci.*, 7(8), 593–596.
- Joughin, I., I. Howat, R. B. Alley, G. Ekstrom, M. Fahnestock, T. Moon, M. Nettles, M. Truffer, and V. C. Tsai (2008), Ice-front variation and tidewater behavior on Helheim and Kangerdlugssuaq Glaciers, Greenland, *J. Geophys. Res.*, 113, F01004, doi:10.1029/2007JF000837.
- Khan, S. A., A. Aschwanden, A. A. Bjørk, J. Wahr, K. K. Kjeldsen, and K. H. Kjær (2015), Greenland ice sheet mass balance: A review, *Rep. Prog. Phys.*, 78(4), 046801.
- Krug, J., J. Weiss, O. Gagliardini, and G. Durand (2014), Combining damage and fracture mechanics to model calving, *Cryosphere*, 8(6), 2101–2117.
- Levermann, A., T. Albrecht, R. Winkelmann, M. Martin, M. Haseloff, and I. Joughin (2012), Kinematic first-order calving law implies potential for abrupt ice-shelf retreat, *Cryosphere*, 6(2), 273–286.
- Liu, Y., J. C. Moore, X. Cheng, R. M. Gladstone, J. N. Bassis, H. Liu, J. Wen, and F. Hui (2015), Ocean-driven thinning enhances iceberg calving and retreat of Antarctic ice shelves, *Proc. Natl. Acad. Sci. U. S. A.*, 112(11), 3263–3268.
- Logg, A., K.-A. Mardal, and G. N. Wells (2012), *Automated Solution of Differential Equations by the Finite Element Method*, Springer, Berlin, doi:10.1007/978-3-642-23099-8.
- Meier, M. F., and A. Post (1987), Fast tidewater glaciers, *J. Geophys. Res.*, 92(B9), 9051–9058.
- Mobasher, M. E., R. Duddu, J. N. Bassis, and H. Waisman (2016), Modeling hydraulic fracture of glaciers using continuum damage mechanics, *J. Glaciol.*, 62(234), 794–804.
- Nick, F. M., C. J. van der Veen, A. Vieli, and D. I. Benn (2010), A physically based calving model applied to marine outlet glaciers and implications for the glacier dynamics, *J. Glaciol.*, 56(199), 781–794.
- Nye, J. F. (1955), Comments on Dr Loewe's letter and notes on crevasses, *J. Glaciol.*, 2(17), 512–514.
- Otero, J., F. J. Navarro, C. Martin, M. L. Cuadrado, and M. I. Corcuera (2010), A three-dimensional calving model: Numerical experiments on Johnsons Glacier, Livingston Island, Antarctica, *J. Glaciol.*, 56(196), 200–214.
- Paterson, W. S. B. (1994), *The Physics of Glaciers*, 3rd ed., Reed Educ. and Prof., Oxford, U. K.
- Pelto, M. S., and C. R. Warren (1991), Relationship between tidewater glacier calving velocity and water depth at the calving front, *Ann. Glaciol.*, 15, 115–118.
- Petrovic, J. J. (2003), Review mechanical properties of ice and snow, *J. Mater. Sci.*, 38(1), 1–6.
- Pollard, D., and R. M. DeConto (2009), Modelling West Antarctic ice sheet growth and collapse through the past five million years, *Nature*, 458(7236), 329–332.
- Pralong, A., and M. Funk (2005), Dynamic damage model of crevasse opening and application to glacier calving, *J. Geophys. Res.*, 110, B01309, doi:10.1029/2004JB003104.
- Reeh, N. (1968), On the calving of ice from floating glaciers and ice shelves, *J. Glaciol.*, 7(50), 215–232.
- Rist, M. A., P. R. Sammonds, S. A. F. Murrell, P. G. Meredith, C. S. M. Doake, H. Oerter, and K. Matsuki (1999), Experimental and theoretical fracture mechanics applied to Antarctic ice fracture and surface crevassing, *J. Geophys. Res.*, 104(B2), 2973–2987.
- Schulson, E. M. (1999), The structure and mechanical behavior of ice, *J. Miner. Met. Mater. Soc.*, 51(2), 21–27.
- Sikonia, W. G. (1982), Finite element glacier dynamics model applied to Columbia Glacier, Alaska, *U.S. Geol. Surv. Prof. Pap. 1258-B*, U.S. Gov. Print. Off., Washington, D. C.
- Smith, R. A. (1976), The application of fracture mechanics to the problem of crevasse penetration, *J. Glaciol.*, 17(76), 223–228.
- Truffer, M., and R. Motyka (2016), Where glaciers meet water: Subaqueous melt and its relevance to glaciers in various settings, *Rev. Geophys.*, 54, 220–239, doi:10.1002/2015RG000494.
- van der Veen, C. J. (1996), Tidewater calving, *J. Glaciol.*, 42(141), 375–385.
- van der Veen, C. J. (1998), Fracture mechanics approach to penetration of surface crevasses on glaciers, *Cold Reg. Sci. Technol.*, 27(1), 31–47.
- van der Veen, C. J. (2002), Calving glaciers, *Prog. Phys. Geogr.*, 26(1), 96–122.
- van der Veen, C. J. (2007), Fracture propagation as means of rapidly transferring surface meltwater to the base of glaciers, *Geophys. Res. Lett.*, 34, L01501, doi:10.1029/2006GL028385.
- van der Veen, C. J. (2013), *Fundamentals of Glacier Dynamics*, 2nd ed., CRC Press, Boca Raton, Fla.
- Vaughan, D., et al. (2013), *Climate Change 2013: The Physical Science Basis. Contribution of Working Group I to the Fifth Assessment Report of the Intergovernmental Panel on Climate Change*, book section 4, pp. 317–382, Cambridge Univ. Press, Cambridge, U. K., and New York.
- Wagner, T. J. W., T. D. James, T. Murray, and D. Vella (2016), On the role of buoyant flexure in glacier calving, *Geophys. Res. Lett.*, 43, 232–240, doi:10.1002/2015GL067247.
- Weertman, J. (1973), Can a water-filled crevasse reach the bottom surface of a glacier?, *Inter. Assoc. Hydrol. Sci. Publ.*, 95, 139–145.